2. Introduction to BRILLOUIN spectroscopy

BRILLOUIN spectroscopy is a well-established optical spectroscopic technique to investigate mechanical as well as magnetic properties of matter (e.g. SANDERCOCK 1982, KRÜGER 1989, HILLEBRANDS 2005). The technique bases on the phenomenon of inelastic laser light scattering, for which the incident photons are scattered by thermally driven elementary excitations in matter, like sound waves (acoustic phonons) or spin waves (magnons) (BRILLOUIN 1922, MANDELSTAM 1926, GROSS 1930, FABELINSKII 1968, CHU 1974, BERNE & PECORA 1976, DIL 1982). Note that BRILLOUIN spectroscopy gives access to hypersonic waves and spin waves without exciting them explicitly by transducers as necessary e.g. for ultrasonic pulse-echo techniques. Since manifold introductory review articles and monographs on BRILLOUIN scattering are available (FABELINSKII 1968, CHU 1974, BERNE & PECORA 1976, DIL 1982, SANDERCOCK 1982, KRÜGER 1989, HILLEBRANDS 2005) and since the current article focuses on scanning BRILLOUIN microscopy, we give only a short introduction to the theoretical background of BRILLOUIN scattering. In a first reading, the sections marked with an asterisk* 2.1 (except figure 2.1 and the related explications) and 2.4 can be skimmed over.

2.1. Scattering of laser light by thermally excited sound waves*

The theory of inelastic scattering of visible light by thermally excited hypersonic waves travelling through transparent matter will be recapitulated within a statistical framework (CHU 1974, BERNE & PECORA 1976). Remember that indeed the continuum of sound waves within condensed matter can be correlated to spatio-temporal fluctuations of the mass density, or more generally, of the strain tensor components (AULD 1973).

Consider a monochromatic laser beam that can be decomposed into planar waves, incident on a dielectric sample. The electric part of each incident planar light wave can be described as:

$$\vec{E}_i(\vec{r},t) = E_0 e^{i(\omega_i t - \vec{k}_i \cdot \vec{r})} \vec{e}_i \,, \qquad (2.1)$$

where $\vec{k}_i$ denotes the wave vector in the medium, $\vec{r}$ the position vector in the sample's coordinate system, ω_i the wave's angular frequency, E_0 the electric field amplitude and $\vec{e}_i$ defines the direction of polarisation. For the sake of simplicity, we assume that within anisotropic matter, the incident and scattered electromagnetic waves represent eigenstates of the electromagnetic field. By this means we exclude effects related to birefringence. The spatially and temporally fluctuating dielectric properties of the sample are described by the dielectric tensor $\underline{\underline{\varepsilon}}(\vec{r},t)$. If the components of the dielectric tensor at optical frequencies fluctuate only spatially, but not temporally, elastic light scattering can occur. In that case, the scattered electromagnetic waves generally propagate along other directions than the incident one while the energy is conserved: $\left\|\vec{k}_i\right\| = \left\|\vec{k}_s\right\|$ and $\vec{k}_i \neq \vec{k}_s$, with $\vec{k}_s$ denoting the scattered wave vector. In the domain of materials science, typical candidates for elastic light scattering processes are polycrystalline materials and nanocomposites possessing optical heterogeneities in the 100 nanometer to micrometer range. Inelastic light scattering occurs if the components of the dielectric tensor at optical frequencies $\underline{\underline{\varepsilon}}(\vec{r},t)$ do not only fluctuate spatially, but also temporally. In this context, two aspects need consideration: the spatially and temporally fluctuating elementary excitations of the sample that couple to its optical properties and the strength of this coupling. The spatio-temporal elementary excitations of the sample can be divided into relaxational fluctuations, like fluctuations of the entropy, and propagating fluctuations, like fluctuations of the mass density (BERNE & PECORA 1976). The corresponding modes are either diffusive or propagating ones. Sound waves (also denoted as acoustic phonons) are generally induced by thermally excited fluctuations of the strain tensor components, which degenerate in ideal liquids to mass density fluctuations. The elasto-optical coupling between the strain fluctuations and the optical fluctuations is described by the Pockels tensor (NYE 1972, VACHER & BOYER 1972). For most materials, the elasto-optical coupling for shear strain is much weaker than that for longitudinal strain (NYE 1972, VACHER & BOYER 1972).

The spatially and temporally fluctuating dielectric tensor at optical frequencies can be described as:

$$\underline{\underline{\varepsilon}}(\vec{r},t) = \left\langle \underline{\underline{\varepsilon}}(\vec{r},t) \right\rangle_{\vec{r},t} + \underline{\underline{\delta\varepsilon}}(\vec{r},t)\,, \tag{2.2}$$

with $\left\langle \underline{\underline{\varepsilon}}(\vec{r},t) \right\rangle_{\vec{r},t}$ denoting the spatially and temporally averaged dielectric tensor and $\underline{\underline{\delta\varepsilon}}(\vec{r},t)$ the fluctuating part of the dielectric tensor. The transversely polarized phonons are responsible for the off-diagonal entries of $\underline{\underline{\delta\varepsilon}}(\vec{r},t)$. The directions of polarization of the incident planar light wave $\vec{e}_i$ and of the chosen inelastically scattered light wave $\vec{e}_s$ yield the components $\delta\varepsilon_{is}$ according to:

$$\delta\varepsilon_{is} = \vec{e}_s \cdot \underline{\underline{\delta\varepsilon}}(\vec{r},t) \cdot \vec{e}_i\,. \tag{2.3}$$

These dielectric fluctuations can be described by the spatio-temporal autocorrelation function of $\delta\varepsilon_{is}$, with V being the scattering volume and Δt the considered time interval:

$$\left\langle \delta\varepsilon_{is}(\vec{r}+\vec{r}\,',t+t')\cdot\delta\varepsilon_{is}(\vec{r},t)\right\rangle_{\vec{r},t} = \frac{1}{\Delta t\cdot V}\int_{-\Delta t/2}^{\Delta t/2} dt \int_V d\vec{r}\;\delta\varepsilon_{is}(\vec{r}+\vec{r}\,',t+t')\cdot\delta\varepsilon_{is}(\vec{r},t) \tag{2.4}$$

The dynamic structure factor $S_{is}(\vec{q},\Omega)$ of the scattered light component travelling in the $\vec{k}_s$-direction results from the spatio-temporal FOURIER transformation of the autocorrelation function of $\delta\varepsilon_{is}$:

$$S_{is}(\vec{q},\Omega) = \int_{-\infty}^{+\infty} dt\; e^{-i\Omega t} \int_V d\vec{r}\; e^{-i\vec{r}\cdot\vec{q}} \left\langle \delta\varepsilon_{is}(\vec{r}+\vec{r}\,',t+t')\cdot\varepsilon_{is}(\vec{r},t)\right\rangle_{\vec{r},t}\,, \tag{2.5}$$

with $\vec{q} = \pm(\vec{k}_s - \vec{k}_i)$ designating the acoustic phonon's wave vector and $\Omega = \pm(\omega_s^{\pm} - \omega_i)$ (with $\omega_s^{\pm}$ being the angular frequencies of the involved scattered electric fields; see section 2.2) its angular frequency. The spectral power density $I_{is}(\vec{q},\Omega) = A_{is}\cdot S_{is}(\vec{q},\Omega)$, which is closely related to the dynamic structure factor, is experimentally accessible by BRILLOUIN spectroscopy. The factor A_{is} depends on the intensity of the incident light. As will be delineated below in a rough overview, the BRILLOUIN lines of the spectral power density are intimately related to the hypersonic properties of the sample, since these lines are due to dielectric fluctuations induced by thermal fluctuations of the strain tensor components (SOMMERFELD 1945, GRIMVALL 1986, LANDAU & LIFSHITZ 1991).

As described in KONDEPUDI & PRIGOGINE (1998), the thermally excited fluctuations of the strain tensor components develop according to the same laws as macroscopic deformations of small amplitude. Within the frame of linear response

theory, the strain $\vec{u}(\vec{q},\Omega)$ can be related to the thermally excited fluctuating elastic force density $\vec{f}(\vec{q},\Omega)$ via the elastic susceptibility tensor $\underline{\underline{\chi}}(\vec{q},\Omega)$, according to:

$$u_k(\vec{q},\Omega) = \chi_{kn}(\vec{q},\Omega)\cdot f_n(\vec{q},\Omega), \text{ with } k,n = 1, 2, 3 . \qquad (2.6)$$

Considering the storing and dissipative parts of the elastic interaction by the symmetric forth rank tensors of the elastic moduli $\underline{\underline{c}} = \{c_{klmn}\}$ and viscosities $\underline{\underline{\eta}} = \{\eta_{klmn}\}$ (with k, l, m, n = 1, 2, 3), the strains $u_k(\vec{q},\Omega)$ evolve with time like damped oscillators. The components of the inverse elastic susceptibilities correspond to (LANDAU & LIFSHITZ 1991, KONDEPUDI & PRIGOGINE 1998):

$$\chi^{-1}_{kn}(\vec{q},\Omega) = \sum_{l,m=1}^{3} c_{klmn} q_l q_m - i\Omega \sum_{l,m=1}^{3} \eta_{klmn} q_l q_m - \rho\Omega^2\delta_{kn}, \qquad (2.7)$$

with ρ denoting the mass density and δ_{kn} the Kronecker symbol. The tensor $\underline{\underline{\chi}}^{-1}(\vec{q},\Omega)$ can be diagonalised in dependence of $\vec{q}$ and Ω, which results in:

$$\underline{\underline{\chi}}(\vec{q},\Omega) = \begin{pmatrix} \chi(1,\vec{q},\Omega) & 0 & 0 \\ 0 & \chi(2,\vec{q},\Omega) & 0 \\ 0 & 0 & \chi(3,\vec{q},\Omega) \end{pmatrix} \qquad (2.8)$$

with

$$\chi(p,\vec{q},\Omega) = \left(q^2\cdot c(p,\vec{q}) - i\Omega q^2\cdot\eta(p,\vec{q}) - \rho\Omega^2\right)^{-1} \qquad (2.9)$$

where $p = 1, 2, 3$ characterizes the polarization state of the sound wave and $c(p,\vec{q})$ denotes the effective elastic modulus for the given wave vector and polarization. The three complex eigenfrequencies $\Omega^*(p,\vec{q}) = \Omega(p,\vec{q}) + i\Gamma(p,\vec{q})$ correspond to the poles of equation (2.9) with:

$$\Gamma(p,\vec{q}) = q^2\eta(p,\vec{q})/2\rho \qquad (2.10)$$

and

$$\Omega(p,\vec{q}) = \sqrt{\Omega_0^2(p,\vec{q}) - \Gamma^2(p,\vec{q})} . \qquad (2.11)$$

Here $\Gamma(p,\vec{q})$ designates the acoustic damping and $\Omega_0(p,\vec{q}) = q\sqrt{c(p,\vec{q})/\rho}$ the eigenfrequencies of the undamped sound waves for a given wave vector $\vec{q}$. The related eigenvectors, i.e. the polarization vectors of the three sound waves, are orthogonal to each other. For p=1, the mode is generally quasi-longitudinally polarized: its polarization vector is almost collinear to the direction of propagation $\vec{q}$ (AULD 1973). Two quasi-transversely polarized modes are described by p=2 and p=3. For elastically isotropic solids, all modes are purely longitudinally or

transversely polarized, i.e. the propagation and polarization vectors are either collinear or perpendicular (AULD 1973). Moreover, the two transversely polarized modes are degenerated for isotropic solids. These shear modes do even not propagate at all in ideal isotropic liquids, where the term 'ideal' implicates the absence of viscoelastic behaviour. In contrast, if the acoustic modes couple to molecular structural relaxations in a liquid, transversely polarized sound modes can be detected at sufficiently high frequencies (CHU 1974, BERNE & PECORA 1976, KRÜGER 1989).

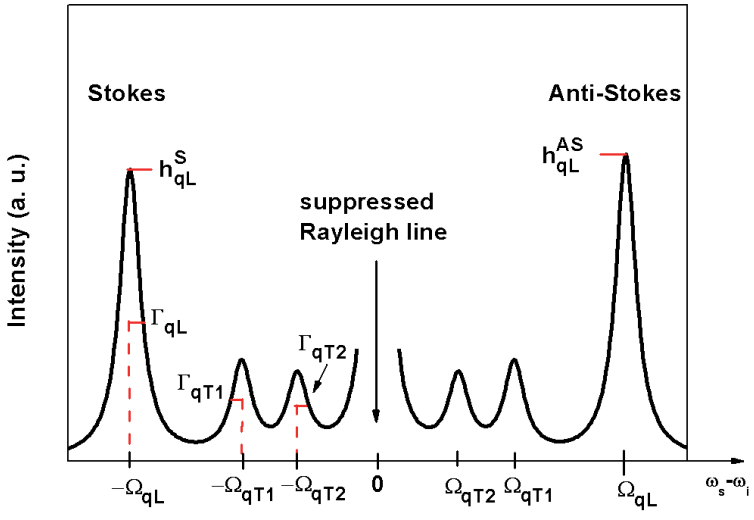

Fig. 2.1. BRILLOUIN spectrum of a homogeneous elastically anisotropic solid containing the BRILLOUIN doublets of the quasi-longitudinally (p=1 or qL) and the two quasi-transversely (p=2, 3 or qT1, qT2) polarized sound modes. (In the following the notation 'qL, qT' will be used.) Angular frequency $\pm\Omega(p,\vec{q})$ *or* $\pm\Omega_{qL,qT1,qT2}$*, hypersonic attenuation:* x_3 *or* $\Gamma_{qL,qT1,qT2}$*, height of STOKES or Anti-STOKES lines:* $h^{S/AS}(p,\vec{q})$ *or* $h^{S/AS}_{qL,qT1,qT2}$*. The central line (suppressed in the figure) corresponds to the RAYLEIGH line, reflecting elastically scattered light and diffusive modes.*

In the classical limit, the fluctuation-dissipation theorem (KONDEPUDI & PRIGOGINE 1998) relates the polarization-independent dynamic structure factor $S(\vec{q},\Omega)$ to the imaginary part of the susceptibility $\mathrm{Im}\left(\chi(p,\vec{q},\Omega)\right)$ by:

$$S(\vec{q},\Omega) = \frac{2k_B T}{\Omega} \sum_{p=1}^{3} \mathrm{Im}\left(\chi(p,\vec{q},\Omega)\right). \qquad (2.12)$$

Note that the opto-acoustic coupling is not part of the so-defined dynamic structure factor, and therefore has to be accounted for by an appropriate prefactor.

In the present rough overview, the relationship between the experimentally accessible spectral power density $I_{is}(\vec{q},\Omega) = A_{is} \cdot S_{is}(\vec{q},\Omega)$ and the elastic susceptibilities, described by equation (2.12), permits us to sense that the angular frequencies $\Omega(p,\vec{q})$ and attenuations $\Gamma(p,\vec{q})$ of the sound waves can be determined from the measured BRILLOUIN spectrum. A typical BRILLOUIN spectrum for a homogeneous anisotropic solid is given in figure 2.1. In the centre of the BRILLOUIN spectrum appears the RAYLEIGH line, corresponding to the elastically scattered light and the diffusive modes. The three BRILLOUIN doublets are positioned symmetrically to the RAYLEIGH line on the horizontal angular frequency axis $\omega_s - \omega_i$. In order to calculate the intrinsic hypersonic attenuations $\Gamma(p,\vec{q})$ the instrumental broadening has to be deconvolved from the measured BRILLOUIN spectrum. The angular frequency and attenuation correspond to the position and the half width at half maximum of the BRILLOUIN lines, respectively. The statistical error of the hypersonic angular frequency typically lies in the one-tenth of percent regime, whereas that of the attenuation is larger by roughly a factor of 10. An increasing half width at half maximum of the BRILLOUIN lines indicates a decreased lifetime of the considered phonon mode $(p,\vec{q})$. The here described lifetime of the phonon (or temporal attenuation of a sound wave) and the spatial attenuation of a sound wave known from ultrasonic investigations are related by the sound velocity. For a very small temporal hypersonic attenuation, i.e. $\Gamma \ll \Omega_0$, the angular frequency Ω is not renormalized by the attenuation (see equation (2.11)). Several

mechanisms are known to contribute to the hypersonic attenuation, like structural relaxation processes with their main relaxation frequencies in the GHz regime (BERNE & PECORA 1976, KRÜGER 1989).

2.2. The kinematic approach

In the frame of a quantum-mechanical description, BRILLOUIN scattering results from inelastic scattering of light photons by acoustic phonons. Applying the law of conservation of energy to this scattering process allows one to relate the hypersonic angular frequency of the phonons Ω to the angular frequencies ω_i and ω_s of the incident and scattered light, respectively, according to:

$$\hbar\omega_s^{\pm} = \hbar\omega_i \pm \hbar\Omega \,. \tag{2.13}$$

The sign '+' corresponds to the annihilation of phonons (Anti-STOKES scattering), and the sign '-' to the creation of phonons (STOKES scattering) (see figure 2.1 in section 2.1). The energy transfer between an incident light photon and an acoustic phonon equals to about 10^{-5} of the photon's energy. Since typical frequencies of visible light are about $5\cdot10^{14}$ Hz, the angular frequencies of the involved acoustic phonons are usually in the GHz regime. Similarly the law of conservation of momentum relates the wave vector $\vec{q}$ of the hypersonic wave to the wave vectors $\vec{k}_i$ and $\vec{k}_s$ of the incident and scattered light according to:

$$\vec{k}_s = \vec{k}_i \pm \vec{q} \,. \tag{2.14}$$

A schematic representation of this law is given in figure 2.2. Using the inner scattering angle θ_i, the norm of the wave vector $\vec{q}$ equals to:

$$q = \left\|\vec{q}\right\| = \sqrt{\left\|\vec{k}_s\right\|^2 + \left\|\vec{k}_i\right\|^2 - 2\left\|\vec{k}_s\right\|\cdot\left\|\vec{k}_i\right\|\cos\theta_i} \,. \tag{2.15}$$

Due to the very small energy transfer between phonons and photons, $\left\|\vec{k}_i\right\| = \left\|\vec{k}_s\right\|$ is a valid approximation leading to:

$$q = \sqrt{2\left\|\vec{k}_i\right\|^2 \cdot (1-\cos\theta_i)} = 2\left\|\vec{k}_i\right\| \sin\frac{\theta_i}{2}. \qquad (2.16)$$

If λ_0 denotes the vacuum laser wavelength and n the sample's refractive index, one obtains:

$$q = \frac{4\pi n \cdot \sin(\theta_i / 2)}{\lambda_0}. \qquad (2.17)$$

Note that in BRILLOUIN scattering the acoustic wave vector $\vec{q}$ is selected by adjusting the adequate scattering geometry, and that the phonon's frequency is the usually complex response. As elucidated in section 2.1, in general three acoustic phonons, one quasi-longitudinally polarized and two quasi-transversely polarized are determined for one selected wave vector $\vec{q}$ in an elastically homogeneous solid (AULD 1973).

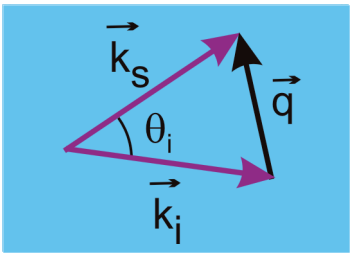

Fig. 2.2. Schematic representation of momentum conservation during an inelastic light scattering process. Sample represented in blue; $\vec{k}_i$, $\vec{k}_s$: incident/scattered light wave vector within the sample; $\vec{q}$: wave vector of the acoustic phonon, and θ_i : inner scattering angle.

For a typical vacuum laser wavelength of $\lambda_0 = 532\,\text{nm}$, the phonon wavelength $\Lambda = 2\pi / q$ equals to some hundred nanometres and is hence of the same order of magnitude as the laser wavelength. Thus, optical elastic scattering, like RAYLEIGH or MIE scattering (BORN & WOLF 1999) in a heterogeneous sample is in most cases accompanied by acoustic RAYLEIGH or MIE scattering (MORSE & INGARD 1968). For

sufficiently small hypersonic attenuation ($\Gamma \ll \Omega$), the phase velocity of the quasi-longitudinally (qL) and quasi-transversely (qT) polarized acoustic modes depends on the phonon wavelength Λ and frequency f according to:

$$v_{qL,\,qT} = \frac{\Omega_{qL,\,qT}}{q} = f_{qL,\,qT} \cdot \Lambda \,. \tag{2.18}$$

Or, using equation (2.17):

$$v_{qL,\,qT} = \frac{f_{qL,\,qT} \cdot \lambda_0}{2n \cdot \sin\left(\theta_i / 2\right)} \,. \tag{2.19}$$

Knowing in addition the sample's mass density, equation (2.19) allows the calculation of the related elastic moduli (AULD 1973):

$$c_{qL,qT} = \rho \cdot v_{qL,qT}^2 \,. \tag{2.20}$$

2.3. Classical scattering geometries

Three common scattering geometries, defining the $\vec{q}$-vector involved in the scattering process, are depicted in figure 2.3. In classical BRILLOUIN spectroscopy, a typical scattering volume is about 10^{-14} m^3 . The 90N scattering geometry, shown in figure 2.3a, is a commonly used scattering geometry due to its easy alignment as $\theta_i = \theta = 90°$, where θ denotes the outer scattering angle (i.e. the angle between the incident and scattered light beam outside the sample). Similarly easy to handle is the backscattering geometry depicted in figure 2.3b, with $\theta_i = \theta = 180°$. The backscattering geometry is especially suitable in case of non-transparent samples as the properties within the scattering volume can often still be probed close to the sample's surface. The major difference to the situation depicted in figure 2.3b is that for a non-transparent sample the scattering volume is much more reduced in the x_3-direction (see also section 3.2). Note that in the backscattering geometry for elastically isotropic samples only information about longitudinally polarized sound waves can be gathered because of symmetry reasons (VACHER & BOYER 1972). During the last years, the backscattering geometry has proven to be highly promising for studying structural processes in dependence of time for transparent

materials (PHILIPP *et al.* 2009, 2011, SANCTUARY *et al.* 2010). Indeed, the large scattering volume in the x_3-direction allows for a comparatively high temporal resolution as BRILLOUIN spectra can be recorded fast. Equations (2.17) and (2.18) allow for calculating the phonon wavelengths and sound velocities for both scattering geometries (using $\theta_i = 90°$ or $\theta_i = 180°$, respectively). The related values, both dependent on the sample's refractive index, are indicated in table 2.1.

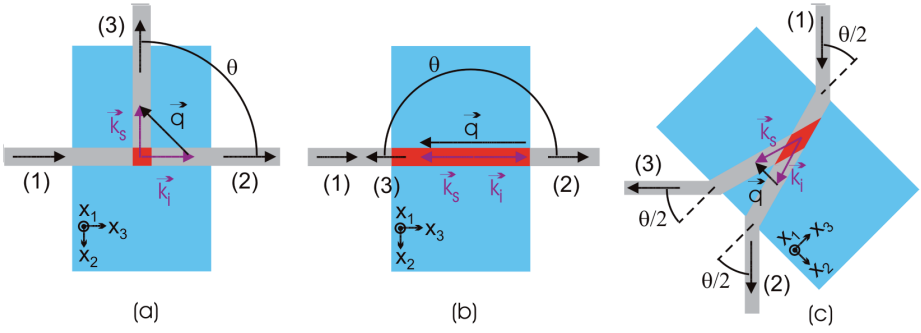

Fig. 2.3. Representation of (a) the 90N scattering geometry, (b) the backscattering geometry, and (c) the θA scattering geometry (here: outer scattering angle $\theta = 90°$). Sample represented in blue, scattering volume in red. (1) laser beam incident on the sample, (2) laser beam leaving the sample, (3) selected direction of the inelastically scattered light emerging from the scattering volume. $\vec{k}_i$, $\vec{k}_s$: incident and scattered wave vector, $\vec{q}$: wave vector of the acoustic phonon. $\{x_1, x_2, x_3\}$: sample coordinate system.

The θA scattering geometry, with θ being strictly between 0° and 90°, is specifically adapted to many experimental challenges (e.g. KRÜGER *et al.* 1978a, 1981, 1986, KRÜGER 1989). It possesses the special attribute that the adjusted phonon wave vector $\vec{q}^{\theta A}$ is independent of the sample's refractive index n in case of optically isotropic samples. Indeed, applying SNELL's law to figure 2.3c allows for expressing the inner scattering angle θ_i in dependence of the outer scattering angle θ:

$$n \cdot \sin\left(\theta_i / 2\right) = \sin(\theta / 2)\,. \qquad (2.21)$$

Combining equations (2.19) and (2.21) then directly leads to the n-independent sound velocity expression for the θA scattering geometry given in table 2.1. Because of the usually small birefringence of anisotropic samples, the expressions indicated in table 2.1 are also high quality approximations for the phonon wave vector and the sound velocities of optically anisotropic samples, with absolute errors being usually smaller than 0.1% (KRÜGER *et al.* 1986). Hence, this scattering geometry is especially useful if high precision acoustic data are needed for samples of unknown optical properties. For instance it is frequently employed for temperature dependent measurements of samples with an unknown refractive index evolution versus temperature (e.g. KRÜGER 1989, KRÜGER *et al.* 1990, 1994, JIMÉNEZ RIOBÓO *et al.* 1990, PHILIPP *et al.* 2008). As thoroughly described in chapter 3, this scattering geometry is often combined with angle-resolved BRILLOUIN spectroscopy to precisely determine the elastic tensor properties of anisotropic samples. Commonly, an outer scattering angle of $\theta = 90°$ is chosen because of the easy alignment. The corresponding scattering geometry is called the 90A scattering geometry.

Table 2.1. Expressions for the phonon wavelength Λ and the sound velocity $v_{qL,qT}$ for different scattering geometries for optically isotropic samples.

Scattering geometry	90N	backscattering	θA	90A
Phonon wavelength Λ	$\frac{\lambda_0}{\sqrt{2}\cdot n}$	$\frac{\lambda_0}{2n}$	$\frac{\lambda_0}{2\cdot\sin(\theta/2)}$	$\frac{\lambda_0}{\sqrt{2}}$
Sound velocity $v_{qL,qT}$	$f^{90N}_{qL,qT}\cdot\frac{\lambda_0}{\sqrt{2}\cdot n}$	$f^{180}_{qL,qT}\cdot\frac{\lambda_0}{2n}$	$f^{\theta A}_{qL,qT}\cdot\frac{\lambda_0}{2\cdot\sin(\theta$	$f^{90A}_{qL,qT}\cdot\frac{\lambda_0}{\sqrt{2}}$

2.4. Determination of elastic tensor components for anisotropic matter*

Scanning acoustic microscopy applied to inhomogeneous and heterogeneous anisotropic materials only makes sense if in addition to the spatial variations of elastic properties accompanying local symmetry changes are recorded. Otherwise both effects, i.e. spatial symmetry changes and inherent elastic modulus variations, can hardly be discriminated. A purposeful experimental approach consists in the combination of scanning BRILLOUIN microscopy with angle-resolved BRILLOUIN spectroscopy. First a recapitulation of the determination of the elastic modulus tensor is proposed before proceeding to this combined experimental technique in the next section.

As shown in the previous sections, in BRILLOUIN spectroscopy the adjustment of the scattering geometry permits to select a phonon wave vector $\vec{q}$ with a desired direction and norm. Angle-resolved BRILLOUIN spectroscopy allows a comparably easy access to the elastic properties in a given scattering volume for many differently oriented $\vec{q}$'s within one plate-like sample (e.g. KRÜGER *et al.* 1985, 1986, 1990, 1994, 2001). Furthermore, in a homogeneous anisotropic material, this technique yields for a given phonon wave vector $\vec{q}$ at best three sound velocities (AULD 1973). The term 'at best' means that the opto-acoustic coupling coefficients must be so large that sufficiently intense phonon lines appear in the BRILLOUIN spectrum. For a given $\vec{q}$ the related phonon modes are orthogonally polarized, but these polarizations are usually neither purely longitudinal nor purely transversal. The evaluation of a BRILLOUIN spectrum does not immediately lead to the material-describing elastic susceptibility, i.e. the fourth rank elastic modulus tensor.

For moderate or negligible acoustic losses this problem is solved by combining the constituting CHRISTOFFEL equation (AULD 1973) with a statistically representative dataset $\{v(\vec{q})\}$ of measured sound velocities (KRÜGER *et al.* 1986, KRÜGER 1989). The CHRISTOFFEL equation combines the measured $\{v(\vec{q})\}$ with the components of the (6×6) elastic modulus matrix $\{c_{nm}\}$ (VOIGT notation; AULD 1973):

$$\begin{pmatrix} \alpha & \delta & \varepsilon \\ \delta & \beta & \zeta \\ \varepsilon & \zeta & \gamma \end{pmatrix} \cdot \begin{pmatrix} w_1 \\ w_2 \\ w_3 \end{pmatrix} = \rho \cdot v^2(\vec{q}) \cdot \begin{pmatrix} w_1 \\ w_2 \\ w_3 \end{pmatrix}. \tag{2.22}$$

Here, ρ denotes the sample's mass density; the eigenvector $\vec{w} = (w_1, w_2, w_3)^t$, expressed in the symmetry coordinate system $\{y_1, y_2, y_3\}$, gives the 'particle velocity', i.e. the oscillation velocity of a volume of the medium being small compared to the whole sample but large compared to the atomic scale. The particle velocity reflects the acoustic polarization of the acoustic mode related to the sound velocity $v(\vec{q})$. The (3×3)-matrix in equation (2.22) is called the CHRISTOFFEL matrix and is defined for the lowest possible symmetry, the triclinic symmetry, by:

$$\begin{aligned}
\alpha &= c_{11}\ell_1^2 + c_{66}\ell_2^2 + c_{55}\ell_3^2 + 2c_{56}\ell_2\ell_3 + 2c_{15}\ell_3\ell_1 + 2c_{16}\ell_1\ell_2 \\
\beta &= c_{66}\ell_1^2 + c_{22}\ell_2^2 + c_{44}\ell_3^2 + 2c_{24}\ell_2\ell_3 + 2c_{46}\ell_3\ell_1 + 2c_{26}\ell_1\ell_2 \\
\gamma &= c_{55}\ell_1^2 + c_{44}\ell_2^2 + c_{33}\ell_3^2 + 2c_{34}\ell_2\ell_3 + 2c_{35}\ell_3\ell_1 + 2c_{45}\ell_1\ell_2 \\
\delta &= c_{16}\ell_1^2 + c_{26}\ell_2^2 + c_{45}\ell_3^2 + (c_{46} + c_{25})\ell_2\ell_3 + (c_{14} + c_{56})\ell_3\ell_1 + (c_{12} + c_{66})\ell_1\ell_2 \\
\varepsilon &= c_{15}\ell_1^2 + c_{46}\ell_2^2 + c_{35}\ell_3^2 + (c_{45} + c_{36})\ell_2\ell_3 + (c_{13} + c_{55})\ell_3\ell_1 + (c_{14} + c_{56})\ell_1\ell_2 \\
\zeta &= c_{56}\ell_1^2 + c_{24}\ell_2^2 + c_{34}\ell_3^2 + (c_{44} + c_{23})\ell_2\ell_3 + (c_{36} + c_{45})\ell_3\ell_1 + (c_{25} + c_{46})\ell_1\ell_2
\end{aligned} \tag{2.23}$$

where the unit vector $\vec{\ell} = (\ell_1, \ell_2, \ell_3) = \left(\frac{q_1}{q}, \frac{q_2}{q}, \frac{q_3}{q}\right)$ gives the propagation direction of the acoustic wave, expressed in the symmetry coordinate system $\{y_1, y_2, y_3\}$. The matrix representation of the fourth rank elastic modulus tensor for triclinic symmetry is given by:

$$\{c_{nm}\} = \begin{pmatrix} c_{11} & c_{12} & c_{13} & c_{14} & c_{15} & c_{16} \\ c_{12} & c_{22} & c_{23} & c_{24} & c_{25} & c_{26} \\ c_{13} & c_{23} & c_{33} & c_{34} & c_{35} & c_{36} \\ c_{14} & c_{24} & c_{34} & c_{44} & c_{45} & c_{46} \\ c_{15} & c_{25} & c_{35} & c_{45} & c_{55} & c_{56} \\ c_{16} & c_{26} & c_{36} & c_{46} & c_{56} & c_{66} \end{pmatrix}. \tag{2.24}$$

For cubic symmetry the CHRISTOFFEL matrix significantly simplifies and is expressed as follows:

$$\begin{aligned}
\alpha &= c_{11}\ell_1^2 + c_{44}\left(\ell_2^2 + \ell_3^2\right) \\
\beta &= c_{11}\ell_2^2 + c_{44}\left(\ell_1^2 + \ell_3^2\right) \\
\gamma &= c_{11}\ell_3^2 + c_{44}\left(\ell_1^2 + \ell_2^2\right). \\
\delta &= \left(c_{12} + c_{44}\right)\ell_1\ell_2 \\
\varepsilon &= \left(c_{12} + c_{44}\right)\ell_1\ell_3 \\
\zeta &= \left(c_{12} + c_{44}\right)\ell_2\ell_3
\end{aligned} \qquad (2.25)$$

The three-dimensional sound velocity polar diagram for crystals of cubic symmetry is still a three-sheeted hypersuperface, similar to the lower symmetries (AULD 1973, KRÜGER *et al.* 1986, KRÜGER 1989). This is in contrast to the degenerated optical phase velocity surface for crystals of cubic symmetry.

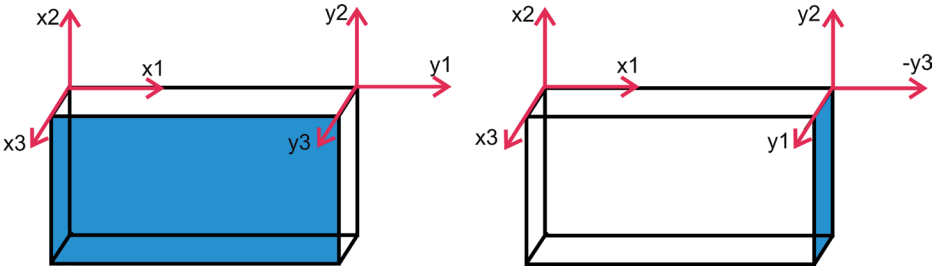

Fig. 2.4. Differently oriented symmetry coordinate systems $\{y_1, y_2, y_3\}$ with respect to the sample coordinate system $\{x_1, x_2, x_3\}$. The blue face denotes a plane parallel to the (y_1, y_2)-plane.

The combination of the 90A scattering geometry with angle-resolved BRILLOUIN spectroscopy is especially suited for determining the elastic tensor of low-symmetry transparent anisotropic materials; a task which is hardly possible by other experimental techniques (e.g. KRÜGER *et al.* 1990, 1994, 2001). A prerequisite for this method is the availability of plate-like samples of the same material, each having a differently oriented symmetry coordinate system $\{y_1, y_2, y_3\}$ with respect

to the sample coordinate system $\{x_1, x_2, x_3\}$ (see figure 2.4). As elucidated in the next chapter, rotating the sample plate around an axis being normal to the sample plane and confining the phonon wave vector $\vec{q}$ within this plane yields the acoustic indicatrix of this sample cut (KRÜGER *et al.* 1985, 1986). The determination of the acoustic indicatrices for a suitable choice of different crystal cuts provides a representative set of elastic data sufficient to calculate, on the base of the CHRISTOFFEL equation, the components of the elastic modulus tensor. This will be exemplarily illustrated in chapter 4 for several crystalline materials.